APPLICATION OF ELECTROCHEMICALLY PREPARED Sn-Co ALLOY POWDERS AS ANODE MATERIAL FOR LITHIUM-ION BATTERIES

Katya Ignatova[1], Toma Stankulov[2]

[1]*University of Chemical Technology and Metallurgy*
Department of Inorganic and Electrochemical Technologies
8 Kliment Ohridski Blvd., Sofia 1797, Bulgaria
[2]*Bulgarian Academy of Sciences*
Institute of Electrochemistry and Energy Systems "Acad. Evgeni Budevski"
G.Bonchev Str., Block 10, 1113 Sofia, Bulgaria
E-mail: katya59ignatova@gmail.com

Received 09 July 2023
Accepted 20 December 2023
DOI: 10.59957/jctm.v59.i2.2024.14

ABSTRACT

The electrochemical behavior of active electrode (anode) materials (AEMs) for lithium-ion battery (LIB), prepared with Sn-Co powders electrodeposited in three different current modes, was investigated. It is shown that AEM with Sn-Co powder, obtained in constant-potential mode, has the highest tin content (82.1 wt. %) and the best performance and stability in operation. The anode material, made with this Sn-Co powder, shows a first-cycle charge capacity of 450 mAh g-1, which decreases to 295 mAh g^{-1} for 10 battery cycles at a current load of 0.8 mA (0.1C). The data also showed that the AEM with Sn-Co powder, deposited in pulse-potential mode, which has the lowest tin content (24.5 wt. % Sn) but the highest dispersity compared to the other powders tested, shows better performance than that of a powder with a tin content of 68.6 wt. %, obtained in constant-current mode. It can be concluded that for the high electrochemical activity of the anode materials, prepared with Sn-Co powders, both the high tin content and the high dispersity and morphological uniformity of the powders are of great importance.

Keywords: Sn-Co powder, electrodeposition, anode material, LIB, cyclic voltammetry.

INTRODUCTION

With the rapidly increasing demand for environmentally friendly and safe energy sources, Li-ion batteries, LIBs are gradually occupying the mainstream market of energy storage devices due to their advantages of high capacity, long cycle life and superior fast recharging ability [1 - 3]. Graphite anodes in LIBs are stable under long-term operation but have one important drawback besides potential safety issues [2]. This is their relatively low theoretical current capacity (372 mAh g^{-1}) compared to that of tin for example (994 mAh g^{-1}) [4]. Therefore, metallic Sn-based anodes have been recommended as one of the most promising alternatives to graphite anode in recent years in both Li-ion and Na-ion batteries [5 - 10]. The main problem for the practical application of pure tin anodes is the large volume changes (about 400 %) during the lithiation and delithiation (insertion/extraction) processes, which lead to a rapid destruction of the electrodes and large irreversible capacity loss during cycling [1, 8, 11]. Alloys of tin with transition metals such as Fe, Co, Ni increase the number of cycles and stabilize the anodes against the occurring volume changes and pulverization during long-term operation [1 - 3, 12]. Co or Ni atoms have been found to form a matrix around the tin atoms and this structure leads to a decrease in the volume expansion of tin during the electrochemical reactions with lithium in LIBs [1]. In search of opportunities to improve battery performance, many modification strategies have been developed, including size control, alloying, and structural design [1, 3].

Modern research has proven the importance of reducing the particle size of applied anode materials for the qualitative improvement of lithium incorporation and release processes [12 - 17]. Nanostructured Sn-Co alloys, encapsulated in hollow carbon carries [15] or nanostructured Sn-Co alloys, deposited on nanocarbon in the shape of nanospheres [6, 8, 13], nanoneedles [7, 17], or other shape, have been investigated [18, 19]. Sn-Co powders, obtained by mechanical mixing [20], mechanically alloyed Sn-Fe(C) powders [21], Sn-Co(C) composites [22], Sn-Co thin films have also been investigated as anode materials for LIBs. Highly porous Sn-Ni alloys [23], macroporous structures [17] and transition metal alloys deposited on nickel foam [14] have also been investigated. Pulsed electrodeposited Sn-Co alloys have shown high current capacity as an anode in LIB [4, 24].

There is no data to investigate the electrochemical behavior of electrodeposited Sn-Co powders as an anode material in LIBs. An ammonium-fluoride electrolyte was developed by us for the preparation of Sn-Co powders [25]. Data on the elemental, phase composition and surface composition of the powders, as well as on its specific surface when applying three current modes – constant-current, constant-potential and pulse-potential modes have also been reported [26, 27].

The present study aimed to investigate the electrochemical behavior of lithium-ion battery anode materials that were made with Sn-Co powders electrodeposited in different current modes.

EXPERIMENTAL

Sn-Co powders obtaining

Sn-Co powders were electrochemically deposited at room temperature, t = 20°C from an ammonium - fluoride electrolyte with a composition: 70 g L^{-1} NH_4F, 1.5 mL/150 mL c.H_2SO_4, pH = 3.8 - 4.0 with ratios between the main salts ($SnCl_2$ and $CoCl_2$) given in Table 1. The powders were deposited using three different current modes: constant-current (CCM), constant-potential (CPM) and pulse-potential modes (PPM).

Morphological and elemental analysis

The surface morphology of the samples was analyzed by scanning electron microscopy (SEM) using an SEM/FIB LYRA I XMU microscope of the company TESCAN with the following characteristics: electronic source - tungsten heated filament; resolution 3.5 nm at 30 kV; accelerating voltage 200 V up to 30 kV. The microscope is equipped with an EDS detector for quantitative analysis Quantax 200 of the company BRUKER. Spectroscopic resolution at Mn-Kα and 1 kcps 126 eV was used.

The parameters of the corresponding modes (current density for CCM, potential for CPM, pulse frequencies at pulse filling Θ = 0.5 and average cathode potential for PPM), in which the three samples were deposited, as well as their elemental compositions in wt. %, are also given in Table 1.

Fig. 1 shows SEM images of the three samples at two microscopic magnifications. As can be seen from Fig. 1, the powders have very different morphologies. It depends not only on the method of deposition but also on the composition of the powders. The tin-enriched powders obtained in CPM have needle-like, elongated particle shape (Fig. 1(c), (c*)), while those in PPM are fine-crystalline, with a typical dendritic shape (Fig. 1 (b), (b*)). Sn-Co powders deposited in CCM have an irregular shape with an average particle size of about 10 μm, which is between that of the two considered samples (Fig. 1 (a), (a*)).

Table 1. Elemental composition of Sn-Co powders (in wt. %) and current conditions for their electrodeposition in constant-current mode (CCM), constant-potential mode (CPM) and pulse-potential mode (PPM).

Sample	Alloys and their elemental comp. in wt. %	Current mode	Conditions	$SnCl_2/CoCl_2$ ratio in the solution in [mol L^{-1}]
1	$Sn_{68.6}Co_{27.8}O_{3.6}$	CCM	j = 150 mA cm^{-2}	0.1M Sn/0.15MCo
2	$Sn_{24.5}Co_{75.5}$	PPM	f = 1000Hz; E = -0.95V(SCE)	0.3M Co/0.15MSn
3	$Sn_{82.1}Co_{3.6}O_{14.3}$	CPM	E =-1.0V(SCE)	0.3M Co/0.15MSn

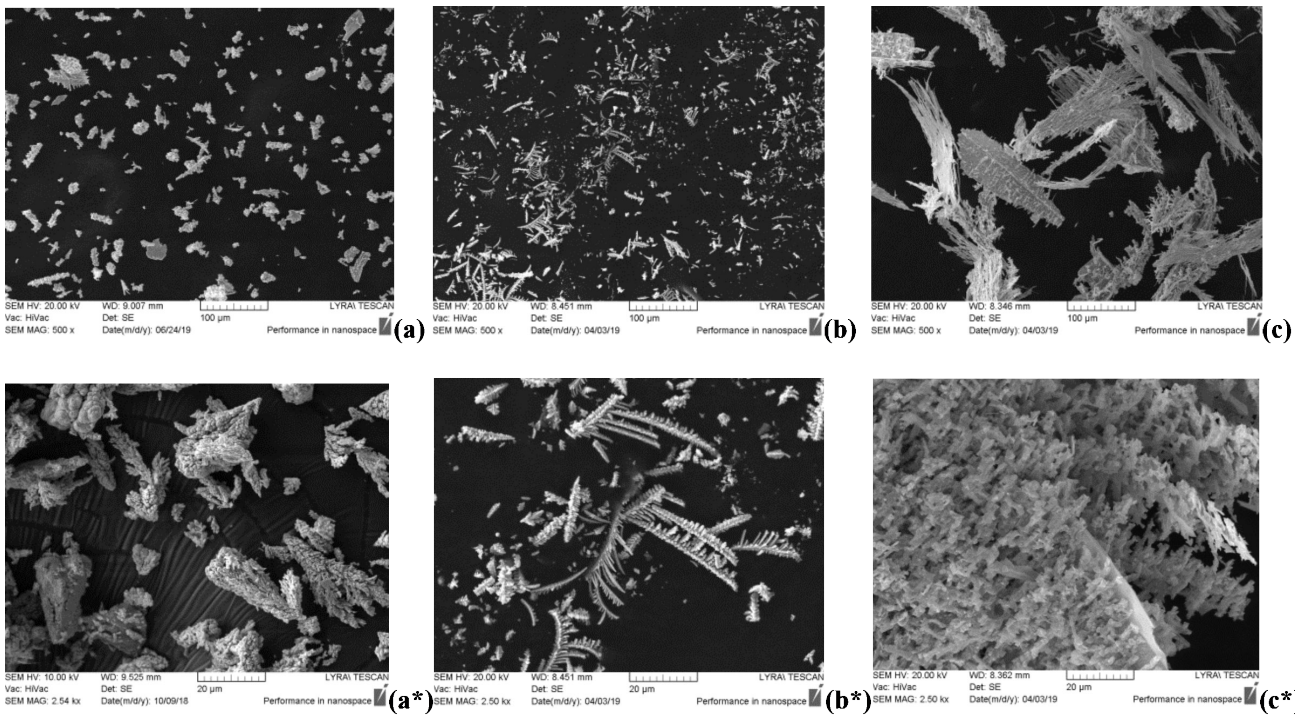

Fig.1. SEM images of the investigated Sn-Co powders (samples 1-3 from Table 1) at two microscopic magnifications: (a) - (c) x500; (a*) - (c*) x2500: (a) - (a*) sample 1; (b) - (b*) sample 2; (c) – (c*) sample 3.

Preparation of anode material

The tested anodes were prepared by mixing 80 % active material, AM (Sn-Co powders) with 10 % teflonized acetylene carbon black (TAB-2) and 10 % binder PvDF (polyvinylidene fluoride), i.e. the active mass is a mixture of AM : TAB2 : PvDF with a weight ratio of 80 : 10 : 10. The prepared powder mixture was dispersed in 2 - 3 drops of solvent 1-methyl-2-pyrrolidine (NMP) to obtain a smooth mass, which was uniformly applied to a copper foil in the shape of a circle with a diameter of 15 mm. The thus prepared electrode was dried at 120°C for 24 hours in a vacuum dryer and pressed under a pressure of 200 kg cm^{-2}.

The electrolyte, used in our tests, is of the type liquid anhydrous aprotic organic solution, which is a mixture of 1M $LiPF_6$ with ethylene carbonate (EC) and dimethyl carbonate (DMC) in a ratio EC : DMC = 1:1 used as solvents for $LiPF_6$. The water content of the electrolyte is below 30 ppm. Lithium foil was used for both counter and reference electrodes. The cell was galvanostatically charged and discharged over a range of current densities from 0.1 to 1.0 mA in a potential window of 0.01 to 3.0 V.

Three-electrode cell

A coin-type CR2032 three-electrode cell (Fig. 2) was assembled in an argon environment in a dry box. This cell was designed to replicate the conditions of a real disk cell, namely, a limited amount of electrolyte and a dense electrode pack. The dense electrode pack was provided by additional pressure on the electrodes from a hollow metal cylinder - a piston (6) through a spring (5). The advantage of this cell is in the repeated and easy assembly and disassembly when conducting the electrochemical studies of the electrodes. Another main advantage of the cell is the presence of a Li/Li+ reference electrode, which allows simultaneous monitoring of the change in the potentials of both electrodes during the electrochemical experiment. A fiberglass separator (2) is placed on the negative electrode. On top of the lithium (1) and the separator (2) lies an insulating cylinder (7), in which the investigated active anode material (8) applied as a paste on a conductive nickel mesh (9) is placed. The electrode pack is pressed by a metal piston with a spring on it (5). The piston and spring provide tightness of the pack as well as electrical contact between the test electrode and the cell cover.

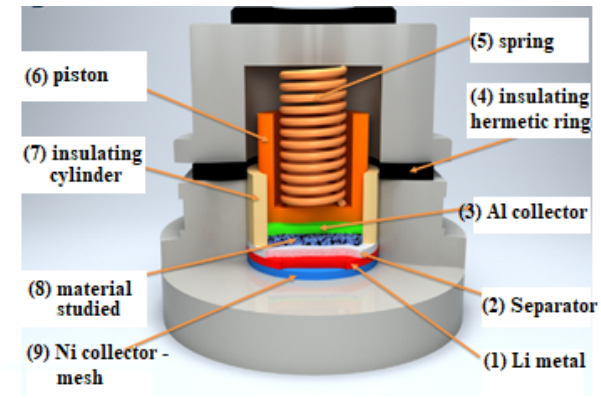

Fig. 2. Three-electrode coin-type cell (the model lithium-ion battery).

Electrochemical tests

Cyclic voltammetry A BA500 Series Battery Analyzer with computer control was used to perform the electrochemical tests of the anode materials. The cycling of the cells with different tested anodes was carried out at room temperature in the voltage range 0.0 - 3.0 V vs. Li^+/Li at different current loads from 0.2 to 1 mA and with a set of 10 hours charge/discharge. The potential window has been adopted in the literature for the study of anode materials. To create quasi-equilibrium scanning conditions (conditions, very close to real battery operation), CV dependencies were recorded at a potential scan rate of 50 to 1000 μV s^{-1}. Using the cyclic voltammetry method (CV) the mechanism of the lithiation (insertion) and delithiation (extraction) processes of Li-ions in and from the tested electrodes was investigated.

Galvanostatic cycling

It involves applying a charge or discharge current to an electrochemical system and measuring the change in potential as a function of time. Maximum and minimum charge and discharge potentials are set, which must be reached in a certain number of cycles. When a current equal to and greater than its open circuit potential is applied to the system, it begins to charge. This causes the lithium ions embedded in the anode to be extracted and the cell potential rises to the set upper charge limit. Exceeding this limit leads to the extraction of a larger than permissible amount of lithium ions and disruption of the stability of the structure of the used active electrode material (AEM). The reverse process occurs when a current is applied, where the cell voltage decreases and energy is consumed. The cell voltage starts to drop until the lower discharge limit is reached. Exceeding this potential limit leads to the occurrence of irreversible changes in the electrode due to the introduction of a larger than permissible amount of lithium ions and disruption of its structure. The data obtained are plotted as a function of potential, E [V] versus time t [h] or versus capacity C (mAh) or specific capacity $C_{spec.}$ (mAh g^{-1}). If the processes are reversible, the charge and discharge curves should be symmetrical. Due to the polarization during discharge and charge, this practically does not happen.

RESULTS AND DISCUSSION

Three samples of Sn-Co powders whit elemental composition and conditions for their deposition given in Table 1 were tested as AEMs. CV dependences were recorded for 3 - 5 battery cycles. The results are described for each of the samples.

$Sn_{68.6}Co_{27.8}O_{3.6}$ - *Sample 1 from Table 1*

Cyclic voltammetric curves

Fig. 3 presents the cyclic voltammetric curves for the processes in a potential window of 0.050÷2.0 V, occurring on an anode material prepared with sample 1 from Table 1. Successive oxidation and reduction peaks are observed in the CV curves, which illustrate the detachment (delithiation) during discharge and incorporation (lithiation) during charging from/into the structure of the anode material.

As can be seen from Fig. 3, in the cathodic direction during the first cycle, the curve has the greatest difference in current compared to the other curves. In this cycle the SEI is formed - a protective film on the surface, which is distinguished by great stability, which is evidenced by the absence of such a dependence in the subsequent 2nd to 5th cycles. In the cathodic branch of the curve up to the 3rd cycle, one reduction peak at 0.6 V and one around 0.2 V are observed (Fig. 3 (a)), and after "stabilization" in the 4th and 5th cycles (Fig. 3 (b)) - only at about 0.3 V. According to literature data [28], the first peak in the cathodic direction (toward more negative potential values) could be due to a topotactic electrochemical reaction of lithium insertion (lithiation) and formation of alloys Li_xSn, according to Eq. (1):

Cathodic direction - lithiation reaction:

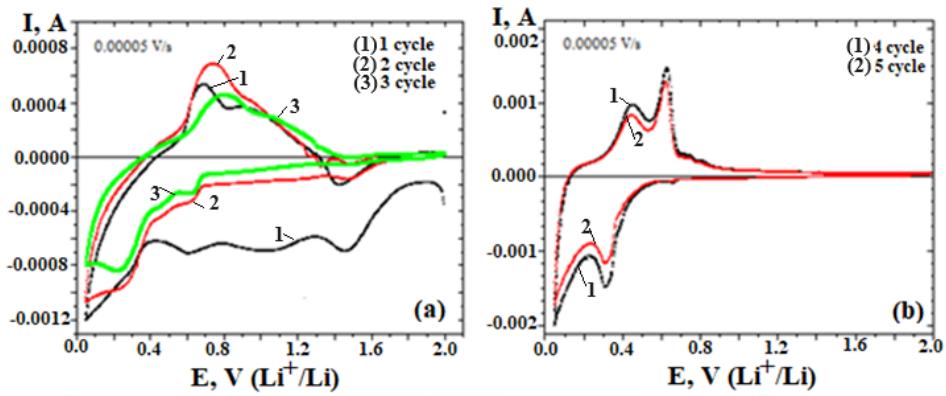

Fig.3. Cyclic voltammetric curves for AEM, prepared with sample 1 from Table 1: (a) for 1-3 cycle and (b) for 4-5 cycle at a scan rate of 50 μV s^{-1}.

$$Co_ySn + xLi^+ + xe^- \rightarrow Li_xSn + yCo \quad (1)$$

Peaks corresponding to potentials below 0.6 are associated with the formation of Li_xSn alloys in which "x" can vary from 7 to 22. The curves at the 4th and 5th cycles are an indication of the stabilization of the charge-discharge processes. The small hysteresis means that the electrochemical reaction taking place is reversible, but also for the irreversible formation of a protective SEI film (Fig. 3 (b)).

In the anodic direction, corresponding to the cathodic, anodic current peaks between 0.7 - 0.8 V are observed. They are the result of decomposition of the various phases of the Li_xSn alloy to the formation of Li^+ according to Eq. (2):

Anodic direction - delithiation reaction:

$$Li_xSn + yCo \rightarrow Sn + xLi^+ + yCo + xe^- \quad (2)$$

Galvanostatic cycling of AEM with sample 1

Understanding the mechanism of lithium incorporation and release in tin is very important in the development of anode materials based on it. It was shown that when a graphite anode material was modified with 20 % tin, several additional reduction and oxidation peaks between 0.6V and 0.8V (vs. Li^+/Li) were observed in the cyclic dependences, which increased with increasing Sn content and correspond to the formation of various LixSn alloys [28]. According to the Li-Sn phase diagram [29] at room temperature eight crystal phases with the following stoichiometric ratios are possible: Li_2Sn_5, LiSn, Li_7Sn_3, Li_5Sn_2, $Li_{13}Sn_5$, Li_7Sn_2 и $Li_{22}Sn_5$. It was established that each alloy is electroactive at different potentials: Li_2Sn_5 - 0.86 V (0.66 V); LiSn - 0.54 V ; Li_7Sn_3 - 0.53 V; Li_5Sn_2 - 0.51 V; $Li_{13}Sn_5$ - 0.4 V; Li_7Sn_2 - 0.34 V; $Li_{17}Sn_4$ - 0.2 V; $Li_{22}Sn_5$ - 0.01 V [28].

In order to evaluate the qualities of the obtained AEMs for application in real electrochemical systems, the behavior of the material was studied under two current loads (0.2 mA and 0.4 mA) for a total of 20 charge/discharge cycles. A standard procedure was used, which included continuous galvanostatic cycling of the test sample under standard conditions, upper and lower cycling limits, and set discharge and charge current. In order to compare the data with those of other authors, the following method of operation was adopted: discharge and charge current 1:1, discharge current 0.1 C (10 hour discharge mode) when the capacity C is the theoretical capacity of the AEM. Only for the first current, the rate of discharge and charge is 0.1 C, calculated according to the mass of the inserted powder. The next current load is recalculated against the same mass against the standard cycling rate of 0.1 C.

From Fig.4 it can be seen that the charge current capacity decreases from 98 mAh g^{-1} for the first cycle and reaches about 45 mAh g^{-1} for the first 10 cycles and changes little for the next 10. The discharge capacity decreases from 70 to 43 mAh g^{-1} for the first 10 cycles. The results show that the anode material exhibits charge and discharge stability. The closeness of the current efficiency during charging and discharging speak for the stable operation of the anode material during its exploitation.

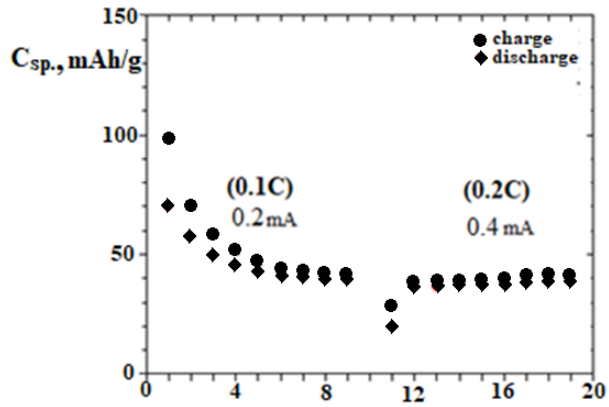

Fig. 4. Dependencies of the specific current capacity for AEM on the number of cycles for two current loads, prepared with sample 1 from Table 1.

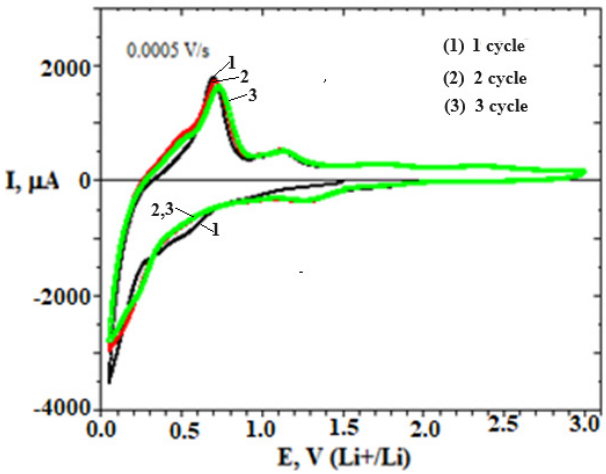

Fig. 5. Cyclic voltammetric curves for AEM, prepared with sample 2 from Table 1.

$Sn_{24.5}Co_{75.5}$ - *Sample 2 from Table 1*

Cyclic voltammetric curves

Fig. 5 shows a CV dependencies describing the processes in a potential window 0.05 - 2.0 V for an anode material prepared with sample 2 from Table 1 at a scan rate of 500 µV s^{-1}. The course of the curves makes it possible to say that in the first cycle, with a charge in the cathodic direction, at potentials around 0.3 - 0.4 V, a stable SEI film is formed.

As can be seen from Fig. 5, in the cathodic direction during the first cycle in the curve one reduction peak is observed at 1.3 V and around 0.6 V. The first one is weak and could be related to impurities present in the AEM. According to the data from the literature, the second peak could be due to a topotactic electrochemical reaction of lithium insertion (lithiation) and formation of alloys such as Li_xSn, according to Eq. (1), mentioned above [28]. In the anodic direction, a current holding at 0.3 V, a clear peak at 0.7 V and a small peak at 1.1 V are observed. The reactions, corresponding to these peaks, are the same as those mentioned above for sample 1 - decomposition reactions (delithiation) of lithium-tin alloys with different composition of lithium (Li_xSn), leading to the formation of Li^+ and Sn according to equation (2). As can be seen from the comparison with Fig. 4, for sample 2 the lithiation and delithiation processes of the material occur at much higher rates compared to sample 1.

Galvanostatic cycling of AEM with sample 2

Fig. 6(A) shows the charge-discharge curves of sample 2 at a current load of 0.4 mA (0.1 C). The cycling was performed in the range determined by the CV measurements and accepted from the literature, namely from 0.1 to 2.0 V. The obtained data are comparable to literature data for similar materials. The selected potential window allows to estimate the full potential of the reversible capacity of the electrochemical system without it undergoing structural changes. On the first cycle, the material shows a charge capacity of 180 mAh g^{-1}. The charge capacity of the 9th cycle is 115 mAh g^{-1}. The obtained data indicate a well-formed and ordered crystal structure of sample 2. The size of the particles, their structure and the presence of porosity in the observed agglomerates have a favorable effect on the demonstrated discharge capacity. On the other hand, the discharge capacities of the material do not exceed 105 mAh g^{-1}. This guarantees the sufficient amount of lithium, necessary to preserve the crystal structure and, as a result, very good reversibility of the material.

Discharge and charge capacity of sample 2 at different current loads

To evaluate the qualities of the obtained AEM for application in real LIBs, its behavior at three different current loads: 0.2, 0.4 and 0.8 mA (respectively 0.05 C, 0.1 C, 0.2 C) was investigated. Fig. 6(B) shows the data for the resulting charge/discharge capacity at different current loads. The charge capacity obtained at 0.4 mA is 123 mAh g^{-1} for the first cycle and decreases to about 75 mAh g^{-1} at the 10th cycle. Similar characteristics are achieved at a current load of 0.2 mA - the capacity is about 92 mAh g^{-1}. It is high and remains stable until the

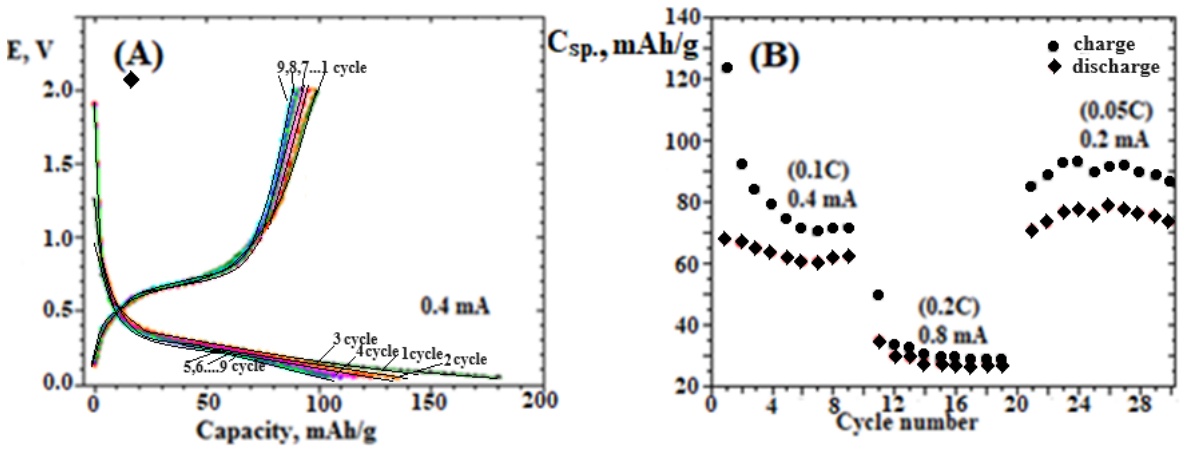

Fig. 6. (A) - Charge/discharge characteristics; (B) - Specific current capacity versus number of cycles for three current loads for AEM prepared with sample 2 from Table 1.

10th cycle. However, the large hysteresis in the curves at both current loads indicates instability of AEM and rapid loss of lithiation and delithiation properties. At the maximum current load for the experiment up to 0.8 mA, a reduction of the capacity from about 50 mAh g^{-1} for the 1st cycle to 29 mAh g^{-1} for the 9th cycle is reached. The low capacities, achieved at the maximum current load, are explained by a low lithium diffusion rate, in which the amount of lithium removed is small. Due to the increased overpotential and earlier reaching the upper limit of the charge transfer rate, there isn't enough time to release the required amount of lithium.

$Sn_{82.1}Co_{3.6}O_{14.3}$ (obtained in Cpm) - *Sample 3 from Table 1*

Cyclic voltammetric curves

Fig. 7 shows the cyclic voltametric curves for AEM, prepared at a scan rate of 500 μV s^{-1} for anode material made with sample 3 from Table 1. The sample shows similar electrochemical behavior to the other two previous AEM. In the cathodic direction, peaks appear at 1.3V and 0.6V, due to an electrochemical reaction related to Sn as a Sn-Co alloy component, involving the formation of Li_xSn alloys and the release of Co according to equation (1) - a lithiation reaction (1) upon charge. The additional peak at 1.32 V disappears after the second cycle and is therefore likely related to a side reaction involving impurities in the AEM. In the anodic direction, two clear peaks similar to those in the curves for samples 1 and 2 are observed - at 0.65 V and a small peak at 0.9 V. The reactions, corresponding to these peaks, are the same as those indicated above for these

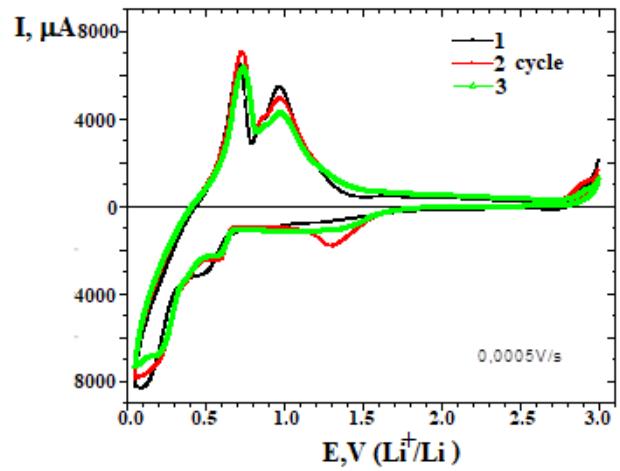

Fig. 7. Cyclic voltametric curves for AEM, prepared with sample 3 from Table 1.

samples - reactions of separation of the Li_xSn alloy to form Li and Sn according to equation (2). The curve has a much smaller hysteresis between the two charge and discharge processes at a 500 μV s^{-1} scan rate. In this case, as well, this indicates that the electrochemical reaction taking place is highly reversible and that a stable SEI film is formed. For sample 3, the lithiation and delithiation processes in the material structure proceed at much higher rates compared to the other two samples (1 and 2 from Table 1). All observed peaks slightly decrease in subsequent cycles after the first cycle. All this is an indication that the studied material could show very good electrochemical behavior, which was also confirmed by the following results.

Discharge and charge capacity of sample 3 at various current loads

To evaluate the qualities of the obtained AEM for application in real LIB, its behavior at two different current loads 0.8 and 1.0 mA was studied, as in Fig. 8 presents the data for the obtained charge and discharge capacities depending on the number of cycles. The average discharge capacity, obtained at a current of 0.8 mA, is significantly higher than the capacity achieved at 1.0 mA.

The recorded charge capacity for 10 cycles of battery operation at a current load of 0.8 mA varies between 450 mAh g^{-1} and 195 mAh g^{-1}. As the current load increased to 1.0 mA, the current capacity decreased from 143 mAh g^{-1} for the first charge cycle to about 92 mAh g^{-1} for the 10th cycle. The achieved high values of the charge capacity are mainly related to the composition of the sample - it has the maximum amount of tin of all samples, which is the electrochemically active part of the alloy, but on the other hand, it is characterized by a specific structure (Fig. 1(c), (c*)).

The summary data of the performed electrochemical tests of the three samples are presented in Table 2. From the data in Table 2 it is clear, that the AEM with the highest tin content (82.1 wt. % Sn, sample 3) shows the best electrochemical performance for the first three cycles and stability under high current loading. This is a sample with the coarsest crystal structure on the other hand. At the same time, the data show that the activity of AEM with the lowest tin content (24.5 wt. % Sn, sample 2) has better characteristics than powder with tin content 68.6 wt. %, sample 1.

From SEM image in Fig.1(b) it can be seen, that powder, deposited in pulse-potential mode has a much more developed surface and a typical dendritic structure. It can be concluded that the reduction of the particle size is indeed of very high importance for the processes of incorporation and release of lithium in the metal matrix. Besides the high content of the active element - tin, an important factor for the electrochemical behavior of the anode material is the small particle size of the metal powders, i.e. their high dispersion.

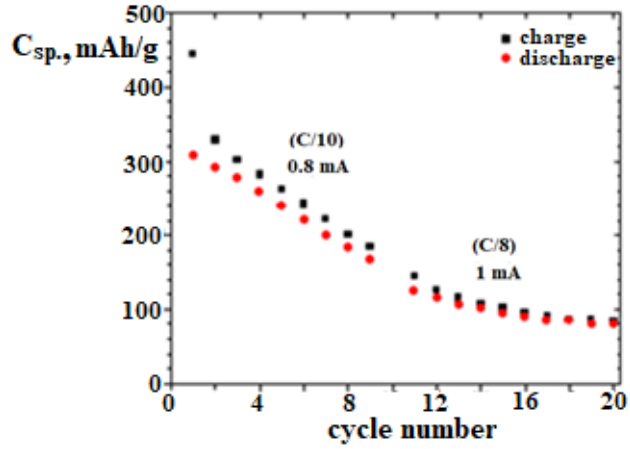

Fig. 8. Dependencies of the specific current capacity for AEM prepared with sample 3 from Table. 1 in terms of the number of cycles for two current loads.

CONCLUSIONS

The following main conclusions can be drawn from the study:

- The electrochemical behavior of active electrode (anode) materials (AEM) for LIBs, prepared with Sn-Co powders electrodeposited in three different current modes, was investigated;
- AEM with Sn-Co powder, deposited in constant-potential mode, has the highest tin content (82.1 wt. %) and the best performance and stability in operation. The anode material, made with this Sn-Co powder, shows a first-cycle charge capacity of 450 mAh g^{-1}, which decreases to 295 mAh g^{-1} for

Table 2. Data on the specific charge ($C_{ch.}$) and discharge capacity ($C_{disch.}$) after the I-th, II-th and III-th cycles (data from the galvanostatic experiment).

Sample	Alloy	Mode	$C_{ch.}$ (I)	$C_{disch.}$ (I)	$C_{ch.}$(II)	$C_{disch.}$ (II)	$C_{ch.}$ (III)	$C_{disch.}$ (III)	I, mA
1	$Sn_{68.6}Co_{27.8}O_{3.6}$	Ccm	99	70	68	57	58	48	0.2
2	$Sn_{24.5}Co_{75.5}$	Ppm	123	68	92	66	83	64	0.4
3	$Sn_{82.1}Co_{3.6}O_{14.3}$	Cpm	450	310	315	290	300	268	0.8

10 battery cycles at a current load of 0.8 mA (0.1C);
- AEM with Sn-Co powder deposited in pulse-potential mode, which has the lowest tin content (24.5 wt. % Sn) but the highest dispersity compared to the other powders tested, shows better performance as anode material than that of a powder with a tin content of 68.6 wt.%, obtained in constant-current mode;
- For the high electrochemical activity of the anode materials, prepared with Sn-Co powders, both the high tin content and the high dispersity and morphological uniformity of the powders are of great importance.

Acknowledgements

The authors are grateful to the Scientific Research Section of University of Chemical Technology and Metallurgy, Sofia for financial support via Projects: 11977FHT_K_I_2020 and 12138_K_I_2021.

REFERENCES

1. H. Ying, W.Q. Han, Metallic Sn-Based Anode Materials: Application in High-Performance Lithium-Ion and Sodium-Ion Batteries Adv Sci (Weinh), 11, 4, 2017: 1700298, Published online 2017 Sep 22. doi: 10.1002/advs.201700298
2. J.M. Tarascon, M. Armand, Issues and challenges facing rechargeable lithium batteries, Nature, 414, 2001, 359.
3. S. Yang, P.Y. Zavalij, M.S. Whittingham, Anodes for lithium batteries: tin revisited, Electrochemistry communications, 5, 7, 2003, 587-590
4. H. Gül, M. Uysal, T. Cetinkaya, H. Akbulut, Preparation of Sn-Co alloy electrode for lithium ion batteries by pulse electrodeposition, Int. J. Hydrogen Energy, 39, 36, 2014, 21414-21419.
5. K. Nishikawa, K. Dokko, K. Kinishita, S.W. Woo, K. Kanamura, Three-dimensionally ordered macroporous Ni–Sn anode for lithium batteries, J. Power Sources, 189, 2009, 726.
6. F. Xin, X. Wang, J. Bai, W. Wen, H. Tian, C. Wang, W. Han, A lithiation/delithiation mechanism of monodispersed MSn_5 (M = Fe, Co and FeCo) nanospheres, J. Mater. Chem. A, 3, 13, 2015, 7170-7178.
7. L. Wang, G. Chen, Q. Shen, G. Li, S. Gua, B. Li, Direct electrodeposition of ionic liquid-based template-free Sn-Co alloy nanowires as an anode for Li-ion batteries, Int. J. Minerals, Metallurgy and Materials, 25, 9, 2018, 1027.
8. X.L. Wang, W.Q. Han, J. Chen, J. Graetz, Single-Crystal Intermetallic M - Sn (M = Fe, Cu, Co, Ni) Nanospheres as Negative Electrodes for Lithium-Ion Batteries, ACS Appl. Mater. Interfaces, 2, 5, 2010, 1548-1551.
9. Zh. Huang, Sh. Ding, Y. Wang, Meiguang Zhang,First-Principles Calculations of SnCo as Potential Anode Materials for High-Performance Lithium-Ion Batteries and Beyond,on-line, electronic available at: https://ssrn.com/abstract=4100245
10. Y. Yui, Y. Ono, M. Hayashi, Y. Nemoto, K. Hayashi, K. Asakura, H. Kitabazashi, Sodium-ion insertion-extraction properties of Sn-Co anodes and Na pre-doped Sn-Co anodes, J. Electrochem. Soc., 162, 2, 2015, A3098-A3102
11. S. Wang, Z. Yi, X. Wang, Q. Sun, Y. Cheng, L.A. Wang, A rational desigh to buffer volume expansion of CoSn intermetallic in lithium and sodium storage: Multicore shell versus monocore-shell, Energy Storage Materials, 23, 2019, 629-635.
12. P.P. Ferguson, A.D.W. Todd, J.R. Dahn, Importance of nanostructure for high-capacity negative electrode materials for Li-ion batteries, Electrochemistry Communications, 12, 2010, 1041-1044.
13. M. Lu, Y. Tian, Y. Li, B. Huang, Synthesis and Characterization of Spherical-Like Tin-Nickel Alloy as Anode for Lithium Ion Batteries, Int. J. Electrochem. Science, 7, 1, 2012.
14. C. Yang, D. Zhang, Y. Zhao, Y. Lu, L. Wang, J.B. Goodenough, Nickel foam supported Sn-Co alloy film as anode for lithium ion batteries, J. Power Sources, 196, 24, 2011, 10673-10678.
15. J. Yang, J. Zhang, X. Zhou, Y. Ren, M. Jiang, J. Tang, Sn-Co nanoalloys encapsulated in N-Doped Carbon Hollow cubes as a high-performance anode material for Lithium-ion batteries, ACS Appl. Mater. Interfaces, 10, 41, 2018, 35216-35223.
16. Z. Du, S. Zhang, Enhanced electrochemical performance of Sn-Co nanoarchitectured electrode for lithium-ion batteries, J. Phys. Chem., 115, 47, 2011, 23603-23609.
17. A.M.W. Elbasiony, Doctoral thesis, Electrodeposition of tin and tin-based alloys from ionic liquids:

Nanowires, thin films and macroporous structures, Nat. Mat. Sciences, Clausthal University of Technology, Egypt, 2015.
18. H. Wang, Y. Sun, X. Zhang, Y. Ding, Y. Wang, X. Wu, Q. Li, Scalable syntesis of SnCo/NC composite as a high-performance anode material for lithium-ion batteries, J. Alloy Comp., 775, 2019, 975-981.
19. V. Milanova, I. Markova, M. Piskin, T. Stankulov, T. Petrov, I. Denev, Synthesis and study of carbon-based nanocomposites with Co-Sn nanoparticles for electrode materials, J. Chem. Techn. Metallurgy, 50, 3, 2015, 288-298.
20. Y. Yui, Y. Ono, M. Hayashi, Y. Nemoto, K. Hayashi, K. Asakura, and H. Kitabayashi, Sodium-Ion Insertion/Extraction Properties of Sn-Co Anodes and Na Pre-Doped Sn-Co Anodes, J. Electrochem. Soc., 162, 2, 2015, A3098-A3102.
21. O. Mao, J.R. Dahn, Mechanically alloyed Sn-Fe(-C) powders as anode materials for Li-ion batteries - III. Sn2Fe: SnFe3C active/inactive composites, J. Electrochem. Soc., 146, 2, 1999, 423-427.
22. M.Y. Li, C.L. Liu, M.R. Shi, W.S. Dong, Nanostructure Sn-Co-C composite lithium-ion battery electrode with unique stability and high electrochemical performance, Electrochim. Acta, 56, 8, 2011, 3023-3028.
23. J. Liu, Y. Wen, P.A.van Aken, J. Maier, Y. Yu, Facile syntesis of highly porous Ni-Sn intermetallic microcages with excellent electrochemical performance for Lithium and Sodium storage, Nano Lett., 14, 11, 2014, 6387-6392.
24. K. Ui, Sh. Kikuchi, N. Kumagai, Preparation of Co–Sn alloy film as negative electrode for lithium secondary batteries by pulse electrodeposition method, Journal of Power Sources 196, 2011, 3916-3920.
25. K. Ignatova, M. Alakushev, An effect of NH_4SCN on deposition of Sn-Co and Sn-Ni powders in fluoride-chloride electrolyte, J. Chem. Techn. Metall., 55, 6, 2020, 875-881.
26. M. Alakushev, K. Ignatova, Influence of electrolyte composition and its temperature on the properties of Sn-Co powder, J. Chem. Techn. Metall., 56, 2, 2021, 360-365.
27. K. Ignatova, D. Lilova, L. Vladimirova, M. Alakushev, Electrodeposition of Sn-Co powders by constant and pulse potential mode, J. Chem. Techn. Metall., 56, 5, 2021, 1066-1073.
28. R.A. Huggins, Lithium alloy negative electrodes, J. Power Sources, 81- 82, 1999, 13-19.
29. J. Wang, I.D. Raistrick, R.A. Huggins, J. Electrochem. Soc., 133, 1986, 457.